AIP | Applied Physics Letters

Interlayer magnetic coupling in perpendicular anisotropy L10-FePt based pseudo spin valve

P. Ho, G. C. Han, G. M. Chow, and J. S. Chen

Citation: Appl. Phys. Lett. **98**, 252503 (2011); doi: 10.1063/1.3602320
View online: http://dx.doi.org/10.1063/1.3602320
View Table of Contents: http://apl.aip.org/resource/1/APPLAB/v98/i25
Published by the American Institute of Physics.

Related Articles

Interlayer exchange coupling between [Pd/Co] multilayers and CoFeB/MgO layers with perpendicular magnetic anisotropy
Appl. Phys. Lett. 101, 242403 (2012)

Magnetotransport properties of dual MgO barrier magnetic tunnel junctions consisting of CoFeB/FeNiSiB/CoFeB free layers
Appl. Phys. Lett. 101, 232401 (2012)

Depth-selective electronic and magnetic properties of a Co2MnSi tunnel magneto-resistance electrode at a MgO tunnel barrier
Appl. Phys. Lett. 101, 232403 (2012)

Exchange-biased magnetic tunnel junctions with antiferromagnetic ε-Mn3Ga
Appl. Phys. Lett. 101, 232402 (2012)

Anisotropic magnetoresistance in topological insulator Bi1.5Sb0.5Te1.8Se1.2/CoFe heterostructures
AIP Advances 2, 042171 (2012)

Additional information on Appl. Phys. Lett.

Journal Homepage: http://apl.aip.org/
Journal Information: http://apl.aip.org/about/about_the_journal
Top downloads: http://apl.aip.org/features/most_downloaded
Information for Authors: http://apl.aip.org/authors

ADVERTISEMENT

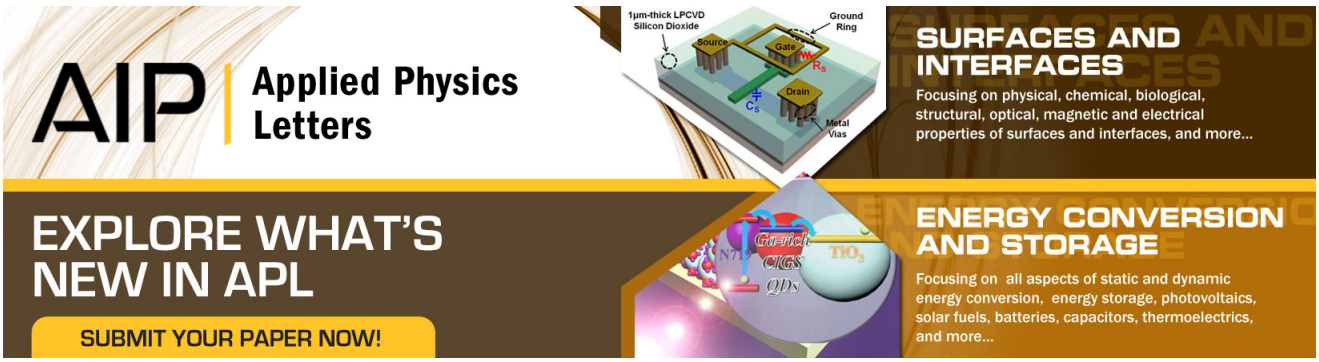

Downloaded 11 Dec 2012 to 137.132.123.69. Redistribution subject to AIP license or copyright; see http://apl.aip.org/about/rights_and_permissions

Interlayer magnetic coupling in perpendicular anisotropy $L1_0$-FePt based pseudo spin valve

P. Ho,[1,2] G. C. Han,[2] G. M. Chow,[1] and J. S. Chen[1,a)]
[1]*Department of Materials Science and Engineering, National University of Singapore, Singapore 117576*
[2]*Data Storage Institute, Agency of Science, Technology and Research (A*STAR), Singapore 117608*

(Received 30 March 2011; accepted 1 June 2011; published online 20 June 2011)

The interlayer coupling effects in $L1_0$-FePt based pseudo spin valve were investigated through the reversal behavior and exchange bias properties of the soft $L1_0$-FePt layer. The magnitude and sign of the exchange bias field were highly dependent on the magnetization state of the hard $L1_0$-FePt layer. In the presence of a fully saturated hard $L1_0$-FePt layer, the exchange bias effect stemmed from interlayer interactions due to possible pinholes, Ruderman–Kittel–Kasuya–Yosida or Néel coupling. With a partially saturated hard $L1_0$-FePt layer, stray fields emanated from the domain walls of the nonuniformly magnetized hard $L1_0$-FePt layer also contributed to the overall coupling strength. © *2011 American Institute of Physics*. [doi:10.1063/1.3602320]

Spin valve systems with perpendicular anisotropy have received much attention due to their intrinsic advantages over in-plane anisotropy for applications in spintronics devices. Pseudo spin valve (PSV) presents an alternative from the standard spin valve in that it does not have an antiferromagnetic (AF) layer to pin the fixed ferromagnetic layer; rather two ferromagnetic (FM) layers with different coercivities are used to control magnetization switching. Achieving independent reversal of the FM layers, in the absence of a pinning AF layer, is difficult as mutual interactions between the FM layers in the PSVs are expected.[1,2] There are several origins to interlayer magnetostatic coupling. Direct interlayer exchange coupling occurs through the pinholes in the spacer layer. Indirect oscillatory coupling arises from Ruderman–Kittel–Kasuya–Yosida (RKKY) interactions. The roughness of the FM/spacer interface can induce Néel orange peel coupling. Furthermore, since magnetization reversal in perpendicular anisotropy thin films takes place through domain nucleation and wall propagation, the nonuniform magnetization distribution induces local stray fields which contributes to dipolar coupling.[3–8] Such magnetostatic interactions will directly affect the independent switching of the magnetic layers and hence the performance of the PSV. Recently, Zha *et al.*[9] observed an exchange bias behavior as part of the coupling effects in $L1_0$ (111)-FePt based PSV with tilted anisotropy. Till date, no such studies have been done on perpendicular anisotropy $L1_0$ (001)-FePt based PSV. In addition, the investigation correlating exchange bias and interlayer magnetostatic interactions had only considered the effects of RKKY and Néel coupling. In this letter, the reversal behavior and exchange bias properties as well as their relationship with the interlayer magnetostatic coupling, further extended to include dipolar coupling, will be investigated for $L1_0$-FePt based PSV.

PSV with the structure MgO(001) substrate/$L1_0$-$Fe_{50}Pt_{50}$ (20 nm)/Ag (2.5 nm)/$L1_0$-$Fe_{50}Pt_{50}$ (5 nm) was deposited using magnetron sputtering system with a base pressure better than 3×10^{-7} Torr. In addition to the different thicknesses, the bottom and top $L1_0$-FePt layers were deposited at 450 °C and 300 °C, respectively to ensure a distinction between their coercivities. Ag spacer layer was deposited at 150 °C and subsequently postannealed at 300 °C. Crystallographic structure was studied by x-ray diffraction (XRD). Magnetic properties were measured by the vibrating sample magnetometer. Surface roughness was investigated using the atomic force microscope (AFM). Magnetic domain configurations were probed with magnetic force microscopy (MFM).

The presence of the superlattice (001) peak (inset of Fig. 1) illustrates that all FePt layers in the PSV displayed well-textured $L1_0$-FePt (001) phase. The top free and bottom fixed $L1_0$-FePt layer possessed coercivities of 1.9 kOe and 3.6 kOe, respectively (Fig. 1). The remanent magnetic configurations of both $L1_0$-FePt layers were studied at the intermediate stages of their reversal process. A +20 kOe field was first applied to fully saturate the sample. Subsequently, a field between −2 and −8 kOe was applied. AFM and MFM images were then taken at zero field to study the remanent magnetic configurations of the layers at different magnetization stages along the first half of the hysteresis loop. Figure 2(a) shows the AFM and MFM images of the PSV after saturation in the +20 kOe field. A poorly contrasted MFM image mapped closely with its corresponding AFM image. It was more of a reflection of the topology of the sample surface, suggesting complete magnetization saturation with spin

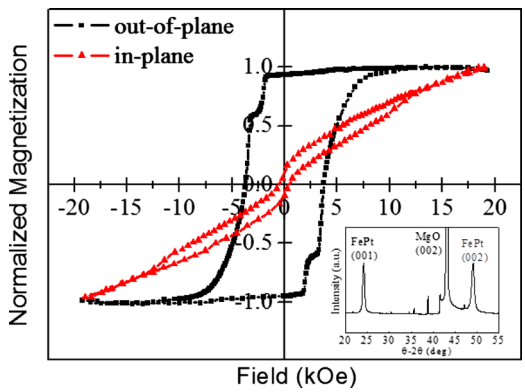

FIG. 1. (Color online) Hysteresis loop of the $L1_0$-FePt (bottom)/Ag/$L1_0$-FePt (top) PSV. The inset shows the θ-2θ XRD spectrum (the unlabelled sharp peaks are inherent of the MgO substrate).

a)Author to whom correspondence should be addressed. Electronic mail: msecj@nus.edu.sg.

 © 2011 American Institute of Physics

Downloaded 11 Dec 2012 to 137.132.123.69. Redistribution subject to AIP license or copyright; see http://apl.aip.org/about/rights_and_permissions

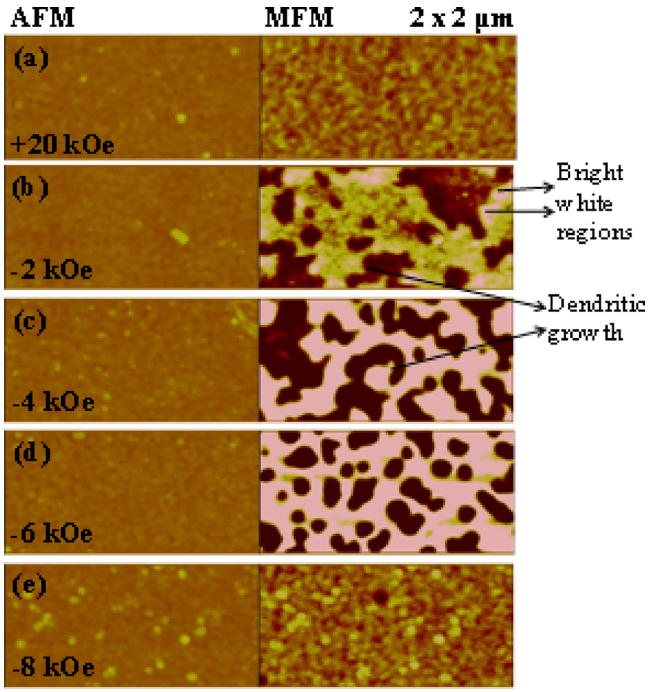

FIG. 2. (Color online) 2×1 μm^2 AFM and MFM images recorded for (a) completely saturated hard and soft $L1_0$-FePt under an applied field of +20 kOe, (b) partial reversal in soft $L1_0$-FePt under an applied field of −2 kOe, (c) partial reversal in hard $L1_0$-FePt under an applied field of −4 kOe, (d) −6 kOe, and (e) close to complete saturation of hard $L1_0$-FePt under an applied field of −8 kOe.

down configuration in both $L1_0$-FePt layers. When a field of −2 kOe was applied [Fig. 2(b)], reversal of the soft $L1_0$-FePt began with the formation of reversed domains (spin up) followed by domain wall propagation (in yellow). The shape of the domain walls was determined by two factors. The first was domain wall elasticity, which tended to straighten the walls; the second was the presence of pinning sites from defects which added irregularity to the shape of the domains. The dendritic shape of the reversed domains observed in the top $L1_0$-FePt was an indication of pinning defects which blocked the propagation path of the reversed domains. This was likely created by the structural disorder due to grain boundaries within the top $L1_0$-FePt layer. High temperature deposition of top $L1_0$-FePt promoted grain formation with diffused Ag preferentially occupying sites along the grain boundaries.[10] Bright white magnetic regions were detected near or along the reversed domain walls of the top $L1_0$-FePt layer. These were due to the decoration of reversed domains in the hard layer by the domain walls in the soft layer. The Bloch walls in the soft layer emanated strong fields to lower the nucleation field in the hard layer. Combined with the external field applied to reverse the soft $L1_0$-FePt layer, the total field generated could be high enough to reach the coercive field of the hard $L1_0$-FePt, bringing about local reversal in the bottom $L1_0$-FePt.[11–13]

At a field of −4 kOe, complete reversal of the top $L1_0$-FePt took place and the MFM probed only magnetic configurations of the bottom $L1_0$-FePt. Figure 2(c) shows bright white regions, indicating similar switching behavior of reversed (spin up) domain formation and wall propagation in the bottom $L1_0$-FePt. A more contrasted image was obtained compared to Fig. 2(b) as a stronger perpendicular magnetic stray field was detected from the thicker bottom $L1_0$-FePt.

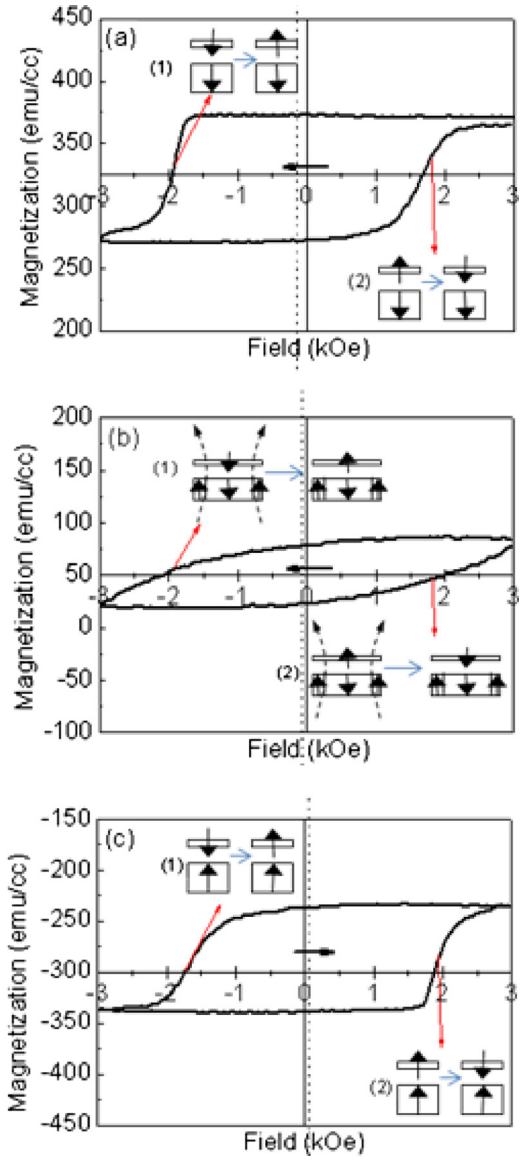

FIG. 3. (Color online) Minor hysteresis loops of the $L1_0$-FePt (bottom)/Ag/$L1_0$-FePt (top) PSV recorded under the influence of the different magnetization state of the bottom $L1_0$-FePt, created through applied field of (a) 0, (b) −4 kOe, and (c) −20 kOe. The dotted line indicates the center of the minor hysteresis loop; the arrow indicates the direction of the shift in the minor hysteresis loop. Insets indicate schematically the influence of bottom $L1_0$-FePt on the reversal of top $L1_0$-FePt as described in the text.

When applied field increased to −6 kOe [Fig. 2(d)], the proportion of bright regions increased with the propagation of spin up domains through the structural disorder. Domain wall shape became spherical instead of dendritic as pinning energy was overcome with greater applied field. Beyond a field of −8 kOe [Fig. 2(e)], close to complete saturation of the bottom $L1_0$-FePt layer occurred, as reflected from the poorly contrasted MFM image.

The influence of the magnetic domain state of the hard $L1_0$-FePt on the magnetization reversal of the soft $L1_0$-FePt was demonstrated through the exchange bias properties of the minor hysteresis loops. A +20 kOe field was applied to fully saturate both $L1_0$-FePt layers in the same spin down direction. A field in the range of (0)–(−20) kOe was then applied to attain different magnetization states of the bottom $L1_0$-FePt. A minor loop below the switching field of the hard magnetic layer, between +3 and −3 kOe, was then cycled.

Downloaded 11 Dec 2012 to 137.132.123.69. Redistribution subject to AIP license or copyright; see http://apl.aip.org/about/rights_and_permissions

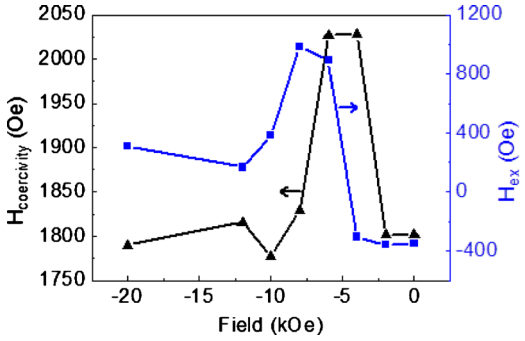

FIG. 4. (Color online) Exchange bias field H_{ex} and coercive field $H_{coercivity}$ of the soft layer vs applied field.

The system behaved as exchange spring magnets, where the minor loops exhibited an exchange bias phenomenon (Fig. 3). The difference between the coercivites in the first and second quadrants was termed the exchange bias field H_{ex}.

With zero applied field, H_{ex} possessed a negative value (Fig. 4). The magnetic moments in both $L1_0$-FePt layers were close to full saturation and aligned in the positive spin down field direction. The small Ag spacer thickness of 2.5 nm and the relatively large interfacial roughness of 1.1 nm made contributions from direct coupling through pinholes, RKKY, or Néel coupling considerable.[3,7–10] When the minor hysteresis loop was carried out, the soft layer (spin down) had to overcome the magnetostatic coupling of the hard layer (spin down) in order to switch to an anti-parallel spin up configuration [inset 1 of Fig. 3(a)] in the second quadrant. In contrast, reversal of the soft $L1_0$-FePt layer (from spin up to spin down) in the fourth quadrant was assisted by the magnetostatic interactions of the hard layer (spin down) [inset 2 of Fig. 3(a)].

With increasing negative field applied, H_{ex} increased and acquired a positive value. Beyond −4 kOe, the hard layer coercivity was reached and significant reversal of the bottom $L1_0$-FePt began. Taking the extreme case of −20 kOe with uniform magnetization of the bottom $L1_0$-FePt in the spin up configuration, the soft layer magnetization experienced greater resistance to switching when the field for the minor loop was applied from −3 to +3 kOe direction [inset 2 of Fig. 3(c)] compared to +3 to −3 kOe [inset 1 of Fig. 3(c)].

H_{ex} peaked in the region of −6 to −8 kOe (Fig. 4). A larger shift in the center of the minor loop toward the positive or negative fields (greater H_{ex}) reflects a greater extent of the interlayer exchange coupling strength.[14] As such, stronger exchange coupling existed between the $L1_0$-FePt layers with partial reversal of the bottom $L1_0$-FePt. In addition to the interlayer magnetostatic coupling effect, there was also the influence of stray field dipolar coupling on the top $L1_0$-FePt, induced by the nonuniform magnetization in the partially switched bottom $L1_0$-FePt. Partial reversal of the hard $L1_0$-FePt resulted in numerous spin up nucleation domains [Fig. 2(c)]. Stray field created at the vicinity of these domain walls promoted dipolar coupling between the hard and soft layers. The spin up field created at the internal border of the spin up domains assisted the formation and propagation of spin up domains in the soft $L1_0$-FePt when the minor loop was swept from +3 to −3 kOe [inset 1 of Fig. 3(b)]. When the minor loop was swept from −3 to +3 kOe, the magnetic reversal of the soft $L1_0$-FePt met with a greater resistance as stray field from the bottom $L1_0$-FePt impeded the propagation of reversed spin down domains in the top $L1_0$-FePt [inset 2 of Fig. 3(b)]. Dipolar coupling strength would be the strongest when the density of the domain walls within the hard layer reached a maximum. This occurred around an applied field of −4 kOe, as seen from the large domain wall area in Fig. 2(c). The magnetostatic coupling strength would be the strongest upon complete saturation of the hard layer at −10 kOe and beyond. The overall coupling strength, being an interplay of stray field dipolar coupling and interlayer magnetostatic interactions, resulted in H_{ex} peaking in the applied field region of −6 to −8 kOe.

A peak in $H_{coercivity}$ also occurred with applied field in the region of −4 to −6 kOe (Fig. 4). The stray field emanating from the partially switched hard $L1_0$-FePt layer created a replication of domains from the hard to the soft $L1_0$-FePt layer. This magnetic disorder impeded domain wall propagation within the soft layer. A larger applied field was needed for the domain walls in the soft $L1_0$-FePt layer to overcome the domain wall pinning and propagate across the stray field pattern.

With complete saturation of the bottom $L1_0$-FePt [Figs. 3(a) and 3(c)], the minor loops exhibited high remanence and rapid magnetic reversal near the coercive field. For an ideal infinite thin film with complete saturation, single domain existed and no stray field was contributed by the bottom $L1_0$-FePt. Hence, dipolar interaction between the $L1_0$-FePt layers was minimized and stronger decoupling was achieved. With partial reversal of the bottom $L1_0$-FePt, the minor loop exhibited sheared behavior and low remanence [Fig. 3(b)]. The switching mechanism of the soft $L1_0$-FePt became more complex as the fringing field from the hard $L1_0$-FePt domain walls caused the domain nucleation field to be locally reduced in the soft $L1_0$-FePt.[13] As such, domain formation occurred nonuniformly within the softer $L1_0$-FePt and over a larger range of applied field.

This work is partially supported by Agency of Science, Technology, and Research (A*STAR), Singapore, SERC Grant No. 092-156-0118 and Ministry of Education, Singapore, Tier 1 funding Grant No. T11-1001-P04.

[1]R. R. Katti, Proc. IEEE **91**, 687 (2003).
[2]R. R. Katti, D. Zou, D. Reed, and H. Kaakani, IEEE Trans. Magn. **39**, 2848 (2003).
[3]V. Baltz, A. Marty, B. Rodmacq, and B. Dieny, Phys. Rev. B **75**, 014406 (2007).
[4]L. Thomas, M. G. Samant, and S. S. P. Parkin, Phys. Rev. Lett. **84**, 1816 (2000).
[5]B. D. Schrag, A. Anguelouch, S. Ingvarsson, G. Xiao, Y. Lu, L. Trouilloud, A. Gupta, R. A. Wanner, W. J. Gallagher, P. M. Rice, and S. S. P. Parkin, Appl. Phys. Lett. **77**, 2373 (2000).
[6]S. Wiebel, J. P. Jamet, N. Vernier, A. Mougin, J. Ferre, V. Baltz, B. Rodmacq, and B. Dieny, Appl. Phys. Lett. **86**, 142502 (2005).
[7]W. S. Lew, S. P. Li, L. Lopez-Diaz, D. C. Hatton, and J. A. C. Bland, Phys. Rev. Lett. **90**, 217201 (2003).
[8]L. Thomas, J. Luning, A. Scholl, F. Nolting, S. Anders, J. Stohr, and S. S. P. Parkin, Phys. Rev. Lett. **84**, 3462 (2000).
[9]C. L. Zha, J. Nogues, and J. Akerman, IEEE Trans. Magn. **45**, 3881 (2009).
[10]P. Ho, G. C. Han, R. F. L. Evans, R. W. Chantrell, G. M. Chow, and J. S. Chen, Appl. Phys. Lett. **98**, 132501 (2011).
[11]A. P. Mihai, J. P. Attané, L. Vila, C. Beigné, J. C. Pillet, and A. Marty, Appl. Phys. Lett. **94**, 122509 (2009).
[12]P. de Person, P. Warin, M. Jamet, C. Beigne, and Y. Samson, Phys. Rev. B **76**, 184402 (2007).
[13]H. W. Fuller and D. L. Sullivan, J. Appl. Phys. **33**, 1063 (1962).
[14]A. Berger, D. T. Margulies, and H. Do, Appl. Phys. Lett. **85**, 1571 (2004).

Downloaded 11 Dec 2012 to 137.132.123.69. Redistribution subject to AIP license or copyright; see http://apl.aip.org/about/rights_and_permissions